Pump-probe photoelectron velocity-map imaging of autoionizing singly excited 4s^{1}4p^{6}np^{1}(n=7,8) and doubly excited 4s^{2}4p^{4}5s^{1}6p^{1} resonances in atomic krypton

Benjamin Doughty, Louis H. Haber, and Stephen R. Leone

Phys. Rev. A **84**, 043433 — Published 31 October 2011

DOI: 10.1103/PhysRevA.84.043433

Pump-Probe Photoelectron Velocity Map Imaging of Autoionizing Singly Excited $4s^1 4p^6 np^1$ (n = 7, 8) and Doubly Excited $4s^2 4p^4 5s^1 6p^1$ Resonances in Atomic Krypton

Benjamin Doughty,[1] Louis H. Haber[1] and Stephen R. Leone

Departments of Chemistry and Physics and Lawrence Berkeley National Laboratory, University of California, Berkeley, California 94720

[1] Present address: Department of Chemistry, Columbia University, New York, New York 1002

Pump-probe photoelectron velocity map imaging, using 27 eV high-harmonic excitation and 786 nm ionization, is used to resolve overlapping autoionizing resonances in atomic krypton, obtaining two-photon photoelectron angular distributions (PADs) for singly and doubly excited states. Two features in the photoelectron spectrum are assigned to singly excited $4s^1 4p^6 np^1$ (n = 7, 8) configurations and four features provide information about double excitation configurations. The anisotropy parameters for the singly excited 7p configuration are measured to be $\beta_2 = 1.61 \pm 0.06$ and $\beta_4 = 1.54 \pm 0.16$ while the 8p configuration gives $\beta_2 = 1.23 \pm 0.19$ and $\beta_4 = 0.60 \pm 0.15$. These anisotropies most likely represent the sum of overlapping PADs from states of singlet and triplet spin multiplicities. Of the four bands corresponding to ionization of doubly excited states, two are assigned to $4s^2 4p^4 5s^1 6p^1$ configurations that are probed to different J-split ion states. The two remaining doubly excited states are attributed to a previously observed, but unassigned, resonance in the vacuum-ultraviolet photoabsorption spectrum. The PADs from each of the double excitation states are also influenced by overlap from neighboring states that are not completely spectrally resolved. The anisotropies of the observed double excitation states are reported, anticipating future theoretical and experimental work to separate

the overlapping PADs into the state resolved PADs. The results can be used to test theories of excited state ionization.

1. Introduction

Autoionizing resonances in atomic and molecular systems are typically short-lived states that decay into the continuum in which they are embedded. The interaction between the continuum and resonance pathways during photoexcitation results in a characteristic interference pattern observed in static spectra known as a Fano line shape.[1-3] The interference provides insight into the interaction between channels, which is obtained by fitting the spectral line shape.[4] The information retrieved from the fit includes the determination of the profile index (q-parameter), which is a measure of the relative oscillator strengths to the modified discrete-state and the band of continuum states, the spectral width, which yields the lifetime of the resonance and contains within it the coupling matrix elements between channels, and the resonance energy. Difficulties in obtaining this information can arise when fitting dense spectral regions or identifying overlapping resonances.[5] Sometimes these limitations can be alleviated with two-color pump-probe experiments that excite the overlapping resonances and subsequently probe them, separating the excited states either in the time[6] or energy domains.

The results of such two-photon experiments also allow for a determination of excited state photoelectron angular distributions (PADs), which can provide the ratio of radial dipole matrix elements that connect the excited state to the outgoing continuum electron partial waves and the phase shift difference between the partial waves.[6-17] Thus, the composition of outgoing electron partial waves in the measured PADs carry with them information on the excited and

final state wavefunctions. The PAD also contains information related to the free electron-ion scattering process, which can describe the interaction of the excited states with neighboring resonances. Thus, by measuring two-photon PADs from multielectron atomic targets, a comparison of results with theoretical models of electronic excitation and photoionization can be made.

The experiment reported here makes use of laser-based high-order harmonics to resonantly pump the $4s^1 4p^6 np^1$ (n = 7, 8) autoionizing states in atomic Kr, which are henceforth referred to as 7p and 8p states for simplicity. For each value of n, there are two optically allowed transitions to J = 1 excited states of differing spin multiplicities in LS-coupling; the lower energy configuration is a triplet and the higher energy configuration is a singlet. The LS-coupled singlet and triplet states can be represented in a *jj*-coupling scheme as $(1/2,3/2)_1$ and $(1/2,1/2)_1$, respectively, although the *jj*-coupled descriptions are not used in the remainder of this report. The singlet and triplet configurations of the 7p and 8p states are not resolved in high-resolution spectra[18-21] and are typically referred to as the singlet state configuration.[22, 23] The 7p and 8p states lie 26.80 eV and 27.03 eV above the $^1S_0$ ground state, respectively.[18-23] In this energetic region several double excitation states that converge to $4s^2 4p^4 5s^1$ ion cores are reported.[18-21] Specifically, signals attributed to $4s^2 4p^4 5s^1 6p^1$ double excitation states are populated and ionized to $4s^2 4p^4 5s^1 (^4P_J)$ ion states. These two-electron double excitation states are also detected in this experiment, and the ejected photoelectrons are spectrally resolved due to the differences in the ionization energies of the single and double excitation ion states. Two other double excitation state signals are also observed and matched with a previously reported resonance in the vacuum-ultraviolet absorption spectrum.[18, 19] All excited states are ionized by a near-infrared ionization laser pulse centered at 1.57 eV (786 nm), which ejects the outermost electron into the continuum

where it is collected with a velocity map imaging (VMI) spectrometer. A schematic of the relevant energy levels and optically accessible pathways are depicted in Fig 1. The excited states populated in this work decay via autoionization on multiple tens of femtoseconds time scale, based on preliminary time-resolved pump-probe measurements and from static line width data.[24] The results of this experiment focus on a single time delay when the pump and probe pulses are temporally overlapped, which is defined as t = 0 fs.

The PADs from the single excitation states are treated as a sum of the unresolved singlet and triplet configurations. The overlap of these two spin states prevents a quantitative determination of the ratio of radial dipole matrix elements and phase shift difference between the partial waves.[6-17] Theoretical calculations might assist in separating the ionization dynamics of the overlapping states more quantitatively in the future. Additional experimental efforts with enhanced time resolution might succeed in separating the singlet and triplet configurations in the time domain, as was performed on the 6p state of Kr.[6] The observed double excitation features consist of four distinct photoelectron bands, two of which are positively assigned from previous spectral measurements;[18-21] the two remaining features are assigned to a previously observed, but unassigned, resonance in the vacuum ultraviolet absorption spectrum.[18, 19] The PADs for these states are reported and may aid in testing correlated electron theories in the future.

2. Experimental Details

The experimental setup used in this work has been described[6, 8-10, 25, 26] and only the essential aspects will be reviewed here. An amplified Ti:Sapphire (Spectra Physics Spitfire Pro) produces 50 fs, 2.5 mJ pulses at 1 kHz and is split into two arms with a waveplate-polarizer

combination. The 17th harmonic is created by focusing approximately 915 mW average power of the fundamental 788 nm driver pulse into a pulsed jet of Ar. The harmonic order and driver frequency are chosen to resonantly pump the $^1S_0$ ground state of Kr to produce excited and aligned nP$_z$ states (ie: $\Delta J = +1$ and $\Delta M_J = 0$ with linearly polarized light). The harmonic spectrum is centered at 26.76 eV with a spectral width of ~0.3 eV (full width at half maximum) to populate the excited states shown in Fig. 1. The 17th harmonic is selected from the high-harmonic output by use of a homebuilt monochromator consisting of a plane grating, plane mirror and torroidal mirror, which serves to separate and focus the light into an effusive beam of Kr. The ionization pulse, centered at 1.57 eV, with average power of 780 mW, is overlapped in space and time with the harmonic pump pulse and the Kr effusive beam. The probe photon acts on the excited Kr atoms, ejecting electron partial waves of several final angular momenta, which interfere in the continuum to yield the measured PAD. The ejected electrons are projected with an electrostatic lens onto an imaging quality micro-channel plate detector in a particle counting VMI spectrometer.[27] Cylindrical symmetry is maintained by optimization of the laser polarizations with a waveplate to be parallel to the detector face. Evaluation of the inverse Abel transform to retrieve the photoelectron speed and angular distributions is accomplished by use of the pBasex inversion technique.[28] Prior to inversion, the collected images are integrated, symmetrized and rebinned to create the final images in the analysis.

The VMI spectrometer is calibrated by measuring single photon ionization of atoms with well-defined ionization energies, including helium, argon, and xenon. The resulting PADs from the single photon ionization of rare gas atoms are also well documented and agree favorably with the results measured during calibration.[29, 30] The probe laser intensity (estimated to be ~10^{12} W/cm^2) is tuned to eliminate multiphoton ionization of the Kr atoms to any detectable extent.

The low probe laser intensity also precludes strong-field effects that would complicate the analysis.[31] The pressure of krypton in the interaction region is also kept low to avoid spectral pulse shaping of the harmonic pump pulse.[32] Spectral line width data suggest the lifetimes of the 7p and 8p states are 84 fs and 97 fs, respectively, while theoretical predictions place the lifetime of the 7p state in a range of 56 fs to 165 fs.[33, 34] The excited state lifetimes of the 7p and 8p states are faster than can be clearly resolved with the current instrumental time-resolution of approximately 80 fs. This prohibits the use of temporal dynamics to potentially resolve the individual singlet and triplet state PADs in time.[6] Efforts to measure the time-dependent evolution of the double excitation signals also reveal dynamics that occur faster than the present instrumental resolution. There is no statistically significant difference among the time dependent signals of the observed photoelectron bands; thus, relative time scales also cannot be determined with the present time-resolution. Errors bars and quoted uncertainties represent one standard deviation in all instances.

3. Results and Analysis

3.1. Assignment of the Pump-Probe Photoelectron Spectrum

The sum of all the background-subtracted pump-probe photoelectron images collected in the experiment is shown in Fig. 2. The left-hand side of the image in Fig. 2 is the raw data, while the right hand side is the inverted data. The intense spot at the center of the inverted image is an artifact of the inversion, where noise is accumulated to the center of the image.[28] Several distinct rings are observed, which correspond to singly and doubly excited state ionizations;

these rings are best assigned by angle-integrating the photoelectron image to produce the pump-probe photoelectron spectrum.

The angle-integrated photoelectron spectrum is shown in Fig. 3 and plotted versus the electron binding energy. It is observed that at least six distinct photoelectron lines are present, which are labeled as bands numbered from 1 to 6, from lowest to highest electron binding energy (largest to smallest rings in Fig. 2). The six bands observed in the photoelectron spectrum are not easily discerned in the photoelectron image shown in Fig. 2. This is because the intensity of each band is spread out over the angular distribution and has a non-obvious radial dependence with the signal intensity. When the photoelectron image is angle integrated, the intensities from each feature in the image accumulate to yield the photoelectron spectrum in Fig. 3.

Bands 2 and 1 have measured binding energies of 0.73 eV and 0.50 eV, respectively. The expected binding energies for the singly excited 7p and 8p states are 0.72 eV and 0.48 eV,[18, 19, 23, 24] which are in excellent agreement with the presently measured values for band 2 and 1. The assignments and observed electron binding energies of bands 1 and 2 are listed in Table 1. Since each *n*p-state in Kr can be populated in a singlet or triplet spin configuration, the bands corresponding to the 7p and 8p states are most likely the sum of two individual intensities and PADs. This results in the summation of the individual state-resolved PADs with an unknown weighting factor to yield the total observed PAD. Additionally, neighboring bands spectrally overlap with each other, which can further contaminate the PADs of an individual state. The effect of overlapping signal intensity from neighboring states will be quantified after the angular distributions of the single excitation states are presented.

There are least four additional bands that are attributed to double excitation states energetically nearby the 7p and 8p resonances, but these are probed to different final ion states. Allowed double excitation states are those of the form $4s^2 4p^4 n\ell^1 n'\ell'^1$, where $\ell\ell'$ can take on the values of sp, pd, sf, or df.[18, 19] The lowest energy electronic configuration that is accessible is $4s^2 4p^4 5s^1 np^1$. The electrons not excited by the harmonic pulse (ie: the $4s^2 4p^4$ electrons) give a ^3P term (in LS-coupling) in the energetic region excited and probed in this work. This is useful to note because the ion states to which the double excitation states are probed are built upon this term.[22, 23] The doubly excited states are constructed by coupling the ^3P inner electrons with the outer valence $5s^1 np^1$ electrons, while the ion states result from coupling the remaining $5s^1$ electron with the ^3P term. As an example, coupling the $5s^1$ electron to the $4s^2 4p^4(^3P)$ ion state can give rise to the lowest energy ^4P_J ion states.

Bands 3 and 5 have measured electron binding energies of 1.05 eV and 1.35 eV, respectively, corresponding to excitation and subsequent ionization of $4s^2 4p^4(^3P)5s^1 6p^1$ double excitation states to different *J*-split ion states.[21] The $4s^2 4p^4(^3P)5s^1(^4P_{5/2})6p^1$ double excitation state has an expected electron binding energy of 1.31 eV when probed to the final $4s^2 4p^4(^3P)5s^1(^4P_{5/2})$ ion state. Similarly, the $4s^2 4p^4(^3P)5s^1(^4P_{3/2})6p^1$ double excitation state has binding energies of 1.31 eV and 1.03 eV when probed to the $4s^2 4p^4(^3P)5s^1(^4P_{3/2})$ and $4s^2 4p^4(^3P)5s^1(^4P_{5/2})$ ion states, respectively.[18, 19, 21-23] Since two ionization signals can potentially overlap at a binding energy of 1.35 eV, it is not certain if two ionizations signals contribute to the intensity of this feature, or if only one is present. Thus, it is possible that band 5 represents two overlapped signals, specifically, from the ionization of the $4s^2 4p^4(^3P)5s^1(^4P_{5/2})6p^1$ doubly excited state to the $4s^2 4p^4(^3P)5s^1(^4P_{5/2})$ ion state and ionization of $4s^2 4p^4(^3P)5s^1(^4P_{3/2})6p^1$ doubly excited states to the $4s^2 4p^4(^3P)5s^1(^4P_{3/2})$ ion state; the uncertainty in the number of ionization signals that

contribute to band 5 is reflected in the assignment given in Table 1. The good agreement between the measured and expected electron binding energies suggests a positive assignment of bands 3 and 5 to the ionization of $4s^2 4p^4(^3P)5s^1(^4P_J)6p^1$ double excitation states. The potential overlap of the two ionization signals in band 5 will complicate the interpretation of the PAD for this band. The assignments and binding energies for bands 3 and 5 are summarized in Table 1.

Additional states that might also be excited within the pump pulse spectral bandwidth are those with electronic configurations $4s^2 4p^4(^1D)5s^1 5p^1$.[35] Previous measurements observe a resonance with this configuration at 26.95 eV,[35] which has an electron binding energy of 1.03 eV if ionized to the $4s^2 4p^4(^3P)5s^1(^4P_{5/2})$ ion state and 1.31 eV when probed to the $4s^2 4p^4(^3P)5s^1(^4P_{3/2})$ ion state. If probed, the ejected electrons from this state would overlap with the ionization signal from the nearby $4s^2 4p^4(^3P)5s^1 6p^1$ states. Ionization of the $4s^2 4p^4(^1D)5s^1 5p^1$ state to the energetically accessible $4s^2 4p^4(^3P)5s^1$ ion core necessitates that the inner electrons (ie: $4s^2 4p^4(^1D)$) are excited via an electronic transition that changes the core electron spin while simultaneously ionizing the outermost valence electron. Electronic transitions that result in the change of electron spins (ie: spin-flips) are forbidden in LS-coupling, so the contribution to the measured photoelectron spectrum from the $4s^2 4p^4(^1D)5s^1 5p^1$ state is expected to be small, if present at all. The possibility exists that spin-orbit interactions might permit such a transition, but the present experimental results do not directly offer insight into the identity of the residual ion core. Theoretical methods might best address the validity of LS-coupling selection rules for the ionization the states probed in this work.

Bands 4 and 6 are attributed to a spectral feature observed, but not assigned, in the vacuum ultraviolet spectrum of Codling et al.[18, 19] at 26.85 eV (labeled 15 by Codling et al.). If this resonance is ionized to $4s^2 4p^4(^3P)5s^1(^4P_{3/2})$ and $4s^2 4p^4(^3P)5s^1(^4P_{5/2})$ ion states, the ejected

photoelectrons will have electron binding energies of 1.14 eV and 1.42 eV, respectively. These expected binding energies agree reasonably well with the measured binding energies of bands 4 and 6 at 1.22 eV and 1.43 eV, respectively. The largest discrepancy is in the observed binding energy of band 4, which might indicate a different spectral assignment, but since no additional resonances have been reported in this energy region, the signals corresponding to bands 4 and 6 are tentatively attributed to the ionization of resonance 15 of Codling et al.[18, 19]

The low lying double excitation states of the form $4s^2 4p^4 (^3P) 5s^1 5p^1$ are not energetically accessible within the harmonic pump pulse spectral bandwidth.[21] Similarly, states that converge to high lying ion cores such as those with ^2S, ^2D, and ^2P terms are not excited within the spectral bandwidth of the harmonic pulse.[18, 19] Based on the measured vacuum ultraviolet spectra and assignments above, it is reasonable to conclude that the measured pump-probe photoelectron spectrum does not have significant features unaccounted for, other than the dominant features shown in Fig. 3 and summarized in Table 1. Two photon transitions in the probe step are neglected at this level of analysis since no obvious features, based upon the assignment of bands, are observed at higher electron kinetic energies.

To determine the extent and effect of overlapping photoelectron intensity from neighboring states on the measured PADs for the 7p and 8p resonances, the photoelectron spectrum is fit to a sum of Gaussian functions, which allows for the percent composition of each photoelectron band to be estimated. The peak positions of the 7p and 8p resonances are kept fixed while the spectral widths are freely fit. The fitted width parameters do not contain information about the excited state lifetimes since the natural line width of each transition is expected to be smaller[24] than the spectral width of the pump pulse, the probe pulse, and the VMI spectrometer energy resolution. Using a broadband light source and a spectrometer with limited

resolution, it is not expected that a meaningful spectral line width can be obtained, even if the probe-laser/high-harmonic spectral widths and instrumental resolution are deconvolved. To determine the natural line width, it would be more accurate to resolve the decay in time, but this cannot be done with the current instrumental time-resolution. The resulting fits are plotted in Fig. 3 as solid lines below the experimental data. The result of fitting the spectrum suggests that the 8p state (band 1) and the 7p state (band 2) might have a non-negligible signal overlap. The 7p state might also be spectrally overlapped with the neighboring double excitation band 3. To assess the influence of overlapping signals on the single excitation photoelectron bands, energetic regions of interest in the photoelectron spectrum are selected and centered at the electron binding energies of the 7p and 8p bands. The regions of interest are illustrated in Fig. 3 as shaded columns centered on the 7p and 8p photoelectron bands. The width of each region of interest corresponds to the standard deviation of a Gaussian profile assumed for each band. The individual Gaussian fits are integrated over the regions of interest and the percent compositions from the resulting summations are evaluated. It is estimated that ~10% of the 8p band in the region of interest may be due to spectral overlap with the neighboring 7p resonance. Similarly, the contamination of the 7p band is estimated to be ~1% in the region of interest. The PAD from the 7p state is expected to yield accurate anisotropy parameters without additional consideration. After the angular distributions for the 7p and 8p states are obtained, the influence of the 7p state on the 8p PAD will be assessed. It should also be noted that despite the energetic proximity of the 7p and 8p resonances to the double excitation resonances in the excitation spectrum, the addition of a probe photon allows one to resolve the nearby states by using the difference in ionization energies for single and double excited configurations.

The region of the pump-probe photoelectron spectrum where double excitation bands are observed can be fit to at least four discrete spectral bands. Given the overlap of these bands, which is easily recognized in Fig. 3, there is clearly significant contamination of the measured PADs of each band by adjacent bands, limiting the quantitative information that can be obtained. Theoretical calculations would aid in separating the state specific PADs for each band in the observed photoelectron spectrum. Few-femtosecond experimental measurements might also help to resolve the overlapping PADs by resolving the states in the time domain rather than the frequency domain.

3.2. Photoelectron Angular Distributions

The excited states are prepared and probed with linearly polarized light that is fixed parallel to the detector face. The PAD is written as a sum of Legendre polynomials with anisotropy coefficients that contain the dynamical information on the excitation and ionization steps. Specifically, the PADs are given by

$$I(\theta) = \frac{\sigma}{4\pi}[1 + \beta_2 P_2(cos\,\theta) + \beta_4 P_4(cos\,\theta)] \qquad (1)$$

where β_2 and β_4 are anisotropy parameters, P_2 and P_4, are the second and fourth order Legendre polynomials, respectively, and σ is the total ionization cross section for the excited state. The angle, θ, is defined relative to the laser polarization, which is vertically oriented in Fig. 2. The anisotropy parameters for each band are determined by evaluating the weighted sum of the anisotropy parameters at each pixel across the band with the photoelectron spectrum intensity. The width of the regions where the anisotropies are measured correspond to approximately one standard deviation of a Gaussian line shape and this was systematically varied and found not to

influence the results in a statistically observable way. Inversions were carried out including higher order expansion terms (up to P_6) and none were found to statistically alter the results; thus, higher order anisotropy expansion terms are not included, as is expected from a two photon process.

3.2.1. Single Excitation State PADs

The measured anisotropy parameters for the 7p state are $\beta_2 = 1.61 \pm 0.06$ and $\beta_4 = 1.54 \pm 0.16$ while the 8p state gives $\beta_2 = 1.23 \pm 0.19$ and $\beta_4 = 0.60 \pm 0.15$. The anisotropies for each single excitation band are summarized in Table 1; polar plots for each band are given in Fig. 4. To test the assumption that the anisotropy parameters from the 8p state are not significantly altered by the estimated 10% contamination from the 7p state, the measured anisotropy parameters for the 8p state are represented as a weighted sum of the individual 7p and 8p anisotropy parameters. The individual anisotropy parameters for the 7p and 8p state are scaled by their relative intensities over the region of interest for the 8p band. The resulting anisotropies are given by the relationship $\beta_{T,m} = 0.10\beta_{7p,m} + 0.90\beta_{8p,m}$, where $\beta_{T,m}$ is the measured m^{th} order anisotropy parameter in the region of the 8p resonance, $\beta_{7p,m}$ is the anisotropy parameter for the 7p state, which is assumed to be identical over the width of the signal, and $\beta_{8p,m}$ represents the anisotropy parameter for the pure 8p signal (i.e.: if completely spectrally resolved from the 7p state). The assumption that the 7p anisotropy near the band maximum is identical to that at the edge of the band is not strictly correct since the anisotropy can vary across the photoelectron line, but the result still provides a basis for estimating the contamination of the 8p state PAD. Using the relationship given above, it is found that the $\beta_{8p,2} = 1.20 \pm 0.21$ and $\beta_{8p,4} = 0.51 \pm 0.17$,

which, when compared to the measured anisotropies before addition of contaminant anisotropy, is not statistically different. Thus, the anisotropies for the 8p resonance are considered to be representative of the individual 8p resonance. Since the separation of the overlapping 7p PAD from the 8p PAD performed above assumes the anisotropy of the 7p resonance at the peak maximum is the same as the anisotropy at the edge of the photoelectron band, the anisotropy parameters for the 8p state are quoted without modification (ie: not deconvolved); this is done to limit the systematic error that might be included during the deconvolution step.

Since the singlet and triplet configurations of the 7p and 8p states are not resolved in this work, the possibility that the PAD measured for bands 1 and 2 might have a coherent contribution should be assessed. Both states could be excited coherently in the same atom by the broad band harmonic pulse. In fact, the PADs from singlet and triplet ionization should not interfere in the continuum because the ejected electrons have different final spin states. In the limit that LS-coupling adequately describes the ionization step, the two overlapping signals should not give rise to a coherent PAD; instead, the two overlapping PADs add incoherently to yield the measured PAD. In the case of ionization events that flip the electron spin ($\Delta S \neq 0$), which might result because of spin-orbit interactions, the electrons from the singlet and triplet states can interfere and would contribute a coherent portion to the measured PAD. Theoretical calculations might assess the validity of the $\Delta S = 0$ dipole selection rule for the ionization of the singly excited states since LS-coupling may not adequately describe the ionization step.

The spectral overlap of the 7p band with the 8p band might yield a coherent part to the 8p PAD since the electron spins can be identical in the final continuum. The magnitude of the coherent term in the PAD is proportional to the transition dipole matrix elements connecting the ground state to both excited states and the transition dipole matrix elements probing the excited

states to the same final continuum. Given that the 8p band was estimated to be composed of ~10% 7p spectral intensity and this was found not to influence the results in a statistically observable way, the possible coherent term is not expected to influence the results given the present experimental uncertainties.

The 7p and 8p anisotropies can be compared with the previously acquired values for the state resolved 6p anisotropy parameters.[6] To compare the results in a meaningful way, the state resolved anisotropies from the 6p state are weighted by the excitation cross sections[20] for each state (the singlet and triplet) then integrated. This assumes the ionization cross section for the singlet and triplet configurations are the same, which might not be the case since the alignment of the singlet and triplet orbital electron densities are perpendicular to one another.[6, 12, 15, 16] The resulting anisotropies for the 6p state are $\beta_2 = 1.52 \pm 0.13$ and $\beta_4 = 1.08 \pm 0.09$. The 6p anisotropies agree qualitatively with the 7p and 8p anisotropies. In some two-photon ionization experiments that probe aligned targets, the anisotropy parameters can be decomposed into the ratio of radial matrix elements and the phase shift difference between the outgoing electron partial waves.[6, 8, 15, 16] This would allow for a quantitative comparison between the anisotropies of the *n*p resonances. However, since the 7p and 8p states measured here consist of two unresolved singlet and triplet signals and the measured anisotropy parameter represents the weighted sum of the two individual PADs, the decomposition of the anisotropies into these parameters is not possible.

Additionally, the anisotropy parameters are strongly dependent on the ejected electron kinetic energy due to the Coulomb phase shift difference that contributes to the total phase shift difference between outgoing electron partial waves.[17] Since the electron kinetic energies from each band are different, this prevents identifying a physical trend from the anisotropies since

each band will have a different total phase shift difference. The observed anisotropy parameters still provide a basis for which future theoretical calculations can be compared since the measured anisotropies represent the essential physics of the excited state and ionization dynamics. Future experimental and theoretical work can aid in separating the contributions of each electronic configuration to the PAD and eventually resolve the measured total anisotropy into state resolved anisotropies, from which a more detailed analysis can be performed.

3.2.2. Doubly Excited PADs

The doubly excited $4s^2 4p^4 5s^1 6p^1$ state ionizations have measured anisotropy parameters of $\beta_2 = 0.40 \pm 0.38$ and $\beta_4 = -0.01 \pm 0.41$, corresponding to band 3, and $\beta_2 = 0.60 \pm 0.14$ and $\beta_4 = -0.15 \pm 0.23$ for band 5. Bands 4 and 6 yield anisotropy parameters of $\beta_2 = 0.49 \pm 0.17$ and $\beta_4 = -0.16 \pm 0.25$ and $\beta_2 = 0.89 \pm 0.18$ and $\beta_4 = -0.43 \pm 0.13$, respectively. The anisotropies for the double excitation bands are summarized in Table 1 and corresponding polar plots are given in Fig. 4. It is likely that overlapping band intensities contaminate the PADs for each individual double excitation state, which limits the quantitative information that can be extracted from the measured anisotropy parameters.

Qualitatively, the PADs from the double excitation states are more isotropic compared to the PADs measured from the single excitation states. The smaller anisotropies measured might be due to overlaps of each double excitation band by adjacent bands, which could lead to an overall lowering of the anisotropies. The alignment of the excited state relative to the probe laser polarization (ie: parallel or perpendicular) will greatly affect the measured anisotropy parameters, most dramatically in the β_4 parameter.[6, 12, 15, 16] Typically, PADs with zero, or near

zero, β_4 parameters reflect the ionization of unaligned targets. The dipole selection rules require that the excited states studied here are prepared with $J = 1$ and $M_J = 0$ (in any coupling scheme) such that the excited states are aligned relative to the pump pulse polarization, so it is unlikely that the small values of the β_4 anisotropy parameters are due to ionization of an unaligned target. Future experimental and theoretical efforts would help determine the alignment of the doubly excited states and to gain a more quantitative understanding of the PADs. Also, the effect of the overlapping PADs can be taken into consideration and separated to yield the nascent PAD for each state provided the PADs of the overlapped states and each contributing band intensity are known. This might be accomplished with a time-resolved measurement, where the temporal evolution of the individual states might allow for a way to separate the individual contributions.[6] Theoretical calculations should also be able to reconstruct the measured PADs by determination of the individual PADs and weighting factors (cross sections) for each band. Thus, the PADs presented here can provide a sensitive test of future theoretical models of doubly excited states and photoionization.

4. Conclusions

The work presented here populates singly excited $4s^1 4p^6 np^1$ and previously observed doubly excited states in atomic Kr with a single high-order harmonic pump pulse. A near infrared ionization laser pulse probes these excited states to the final continuum where the difference in ionization energy allows for spectral differentiation of the single and double excitation states. The anisotropies for the singly excited 7p and 8p states are reported and regarded as a weighted sum of unresolved singlet and triplet PADs. Future theoretical and

experimental efforts might be able to separate the measured total PADs into state-resolved PADs to gain insight into the excited state and photoionization dynamics for the singlet and triplet configurations of the $4s^1 4p^6 np^1$ autoionizing series in Kr. Four photoelectron bands are observed and assigned to doubly excited states previously reported in the vacuum-ultraviolet photoabsorption spectrum. Congestion of the double excitation bands at high photoelectron binding energies limits the quantitative information about the excited state and ionization dynamics that can be extracted with the present data alone. The results will serve to test future theoretical models of photoionization from doubly excited states, but will also benefit from calculations that might separate the overlapping PADs into state resolved PADs for each double excitation band.

The authors acknowledge many useful and stimulating conversations with Dr. Zhi-Heng Loh. Financial support is provided by the Director, Office of Science, Office of Basic Energy Sciences, Chemical Sciences, Geosciences, and Biosciences Division, U.S. Department of Energy under contract No. DE-AC02-05CH11231.

References

1 U. Fano, Phys. Rev. **124**, 1866 (1961).

2 U. Fano and J. W. Cooper, Phys. Rev. **137**, 1364 (1965).

3 A. R. P. Rau, Phys. Scr. **69**, C10 (2004).

4 B. W. Shore, Phys. Rev. **171**, 43 (1968).

5 F. H. Mies, Phys. Rev. **175**, 164 (1968).

6 B. Doughty, L. H. Haber, C. Hackett, and S. R. Leone, J. Chem. Phys. **134**, 094307 (2011).

[7] R. L. Chien, O. C. Mullins, and R. S. Berry, Phys. Rev. A **28**, 2078 (1983).

[8] L. H. Haber, B. Doughty, and S. R. Leone, Phys. Rev. A **79**, 031401 (2009).

[9] L. H. Haber, B. Doughty, and S. R. Leone, J. Phys. Chem. A **113**, 13152 (2009).

[10] L. H. Haber, B. Doughty, and S. R. Leone, Molec. Phys. **108**, 1241 (2010).

[11] H. Kaminski, J. Kessler, and K. J. Kollath, Phys. Rev. Lett. **45**, 1161 (1980).

[12] C. Kerling, N. Bowering, and U. Heinzmann, J. Phys. B-At. Mol. Opt. Phys. **23**, L629 (1990).

[13] G. Leuchs and S. J. Smith, Phys. Rev. A **31**, 2283 (1985).

[14] E. Matthias, P. Zoller, D. S. Elliott, N. D. Piltch, S. J. Smith, and G. Leuchs, Phys. Rev. Lett. **50**, 1914 (1983).

[15] O. C. Mullins, R. L. Chien, J. E. Hunter, D. K. Jordan, and R. S. Berry, Phys. Rev. A **31**, 3059 (1985).

[16] O. C. Mullins, R. L. Chien, J. E. Hunter, J. S. Keller, and R. S. Berry, Phys. Rev. A **31**, 321 (1985).

[17] S. J. Smith and G. Leuchs, in *Advances in Atomic and Molecular Physics*, edited by B. Sir David Bates and Benjamin (Academic Press, 1988), Vol. Volume 24, p. 157.

[18] K. Codling and R. P. Madden, Phys. Rev. A **4**, 2261 (1971).

[19] K. Codling and R. P. Madden, J. Res. Nat. Bur. Stand. Sect. A. Phys. Chem. **A 76**, 1 (1972).

[20] D. L. Ederer, Phys. Rev. A **4**, 2263 (1971).

[21] V. L. Sukhorukov, et al., J. Phys. B-At. Mol. Opt. Phys. **40**, 1295 (2007).

[22] Y. Ralchenko, A. E. Kramida, J. Reader, and NIST ASD Team, 2008).

[23] E. B. Saloman, J. Phys. Chem. Ref. Data **36**, 215 (2007).

[24] D. L. Ederer, Phys. Rev. A **4**, 2263 (1971).

[25] D. Strasser, F. Goulay, and S. R. Leone, J. Chem. Phys. **127**, 184305 (2007).

[26] D. Strasser, L. H. Haber, B. Doughty, and S. R. Leone, Molec. Phys. **106**, 275 (2008).

[27] A. Eppink and D. H. Parker, Rev. Sci. Instrum. **68**, 3477 (1997).

[28] G. A. Garcia, L. Nahon, and I. Powis, Rev. Sci. Instrum. **75**, 4989 (2004).

[29] D. M. P. Holland, A. C. Parr, D. L. Ederer, J. L. Dehmer, and J. B. West, Nuclear Instruments & Methods in Physics Research **195**, 331 (1982).

[30] K. T. Taylor, J. Phys. B-At. Mol. Opt. Phys. **10**, L699 (1977).

[31] P. L. Knight, M. A. Lauder, and B. J. Dalton, Phys. Rep.-Rev. Sec. Phys. Lett. **190**, 1 (1990).

[32] D. Strasser, T. Pfeifer, B. J. Hom, A. M. Muller, J. Plenge, and S. R. Leone, Phys. Rev. A **73**, 021805 (2006).

[33] K. Gokhberg, V. Averbukh, and L. S. Cederbaum, J. Chem. Phys. **126**, 154107 (2007).

[34] M. Stener, P. Decleva, and A. Lisini, J. Phys. B-At. Mol. Opt. Phys. **28**, 4973 (1995).

[35] M. Valin and P. Marmet, J. Phys. B-At. Mol. Opt. Phys. **8**, 2953 (1975).

Figure Captions

Fig. 1: Sketch of the electronic states in Kr that are excited and subsequently probed in this work. The excitation, ionization, and relaxation pathways are indicated by arrows. The $^1S_0$ ground state is pumped by the 17th harmonic to simultaneously excite the 7p and 8p singly excited states as well as double excitation states (dbl). Each of the populated states decays with a characteristic autoionization lifetime, given by τ_{ai}. The excited states are probed to a final continuum producing a photoelectron with a kinetic energy, E_K, that is measured in the VMI

spectrometer. The $4s^1 4p^6 np^1$ states are ionized to the $4s^1 4p^6$ continuum, while the double excitation states are probed to *J*-split $4s^2 4p^4 5s^1$ ion cores and are spectrally resolved from the single excitation bands by way of the difference in ionization energies.

Fig. 2: (Color Online) The raw (left hand side) and inverted (right hand side) pump-probe photoelectron images are shown here at a time delay where pump and probe pulses are temporally overlapped. The single excitation bands are roughly indicated on the figure and discussed in more detail in the text. The double excitation signals are also noted, but not individually identified because congestion at low photoelectron energies (small radius) makes it difficult to identify each state in the image. The angle integrated photoelectron spectrum permits the assignment of each feature in the image more quantitatively.

Fig. 3: (Color Online) The angle integrated photoelectron spectrum is plotted here versus the electron binding energy. Experimental data is plotted as a solid line bracketed by a filled area that represented the experimental uncertainty. At least six distinct signals are observed and assigned a band number listed across the top of the figure. To estimate the extent of spectral overlap for the single excitation PADs, the spectrum is fit to a sum of six Gaussian functions (solid lines beneath the experimental data), as described in the text. The highlighted columns centered at the 7p and 8p signals represent the regions of interest used to estimate signal contamination on each resonance and also represent the region where the anisotropy parameters are measured for the 7p and 8p states.

Fig. 4: Polar plots of the photoelectron anisotropy parameters reported in Table 1. The grey shaded regions represent the uncertainties associated with the quoted anisotropy parameters. The laser polarization is vertically oriented in each plot.

Table 1: Summary of the observed photoelectron bands, their spectral assignments, the electron binding energy of each band, and the observed β_2 and β_4 anisotropy parameters is given here. Bands 4 and 6 are tentatively assigned as described in the text.

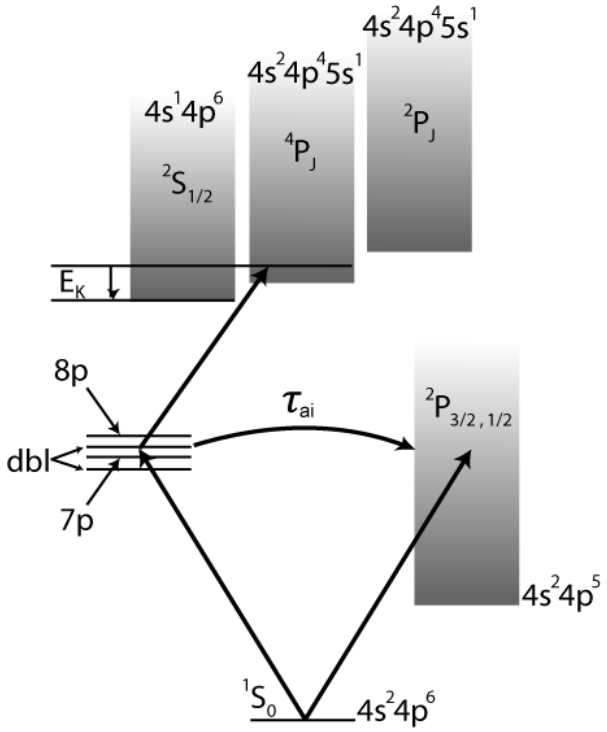
4s²4p⁴5s¹
4s²4p⁴5s¹
4s¹4p⁶
²P_J
⁴P_J
²S_1/2
E_K
8p
τ_ai
²P_3/2 , 1/2
dbl
7p
4s²4p⁵
¹S_0
4s²4p⁶

Fig. 1:

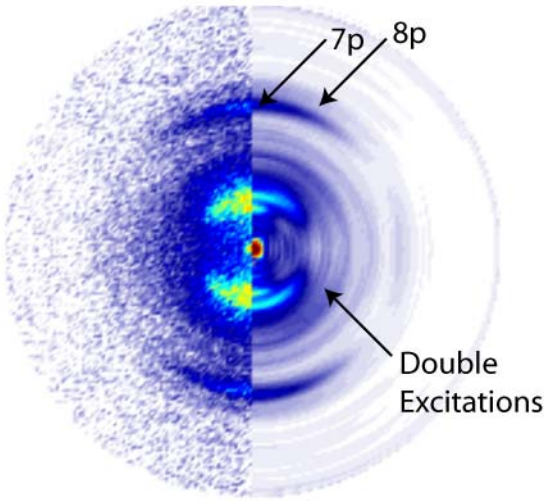

Fig. 2:

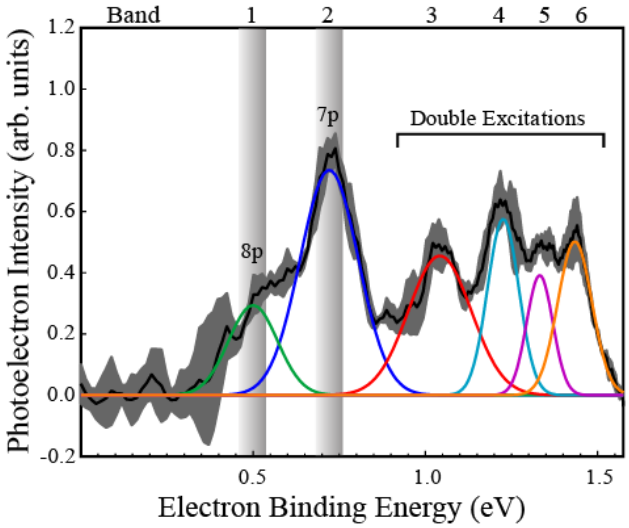
Band
1
2
3
4
5
6
7p
8p
Double Excitations
Photoelectron Intensity (arb. units)
Electron Binding Energy (eV)
1.2
1.0
0.8
0.6
0.4
0.2
0.0
-0.2
0.5
1.0
1.5

Fig. 3:

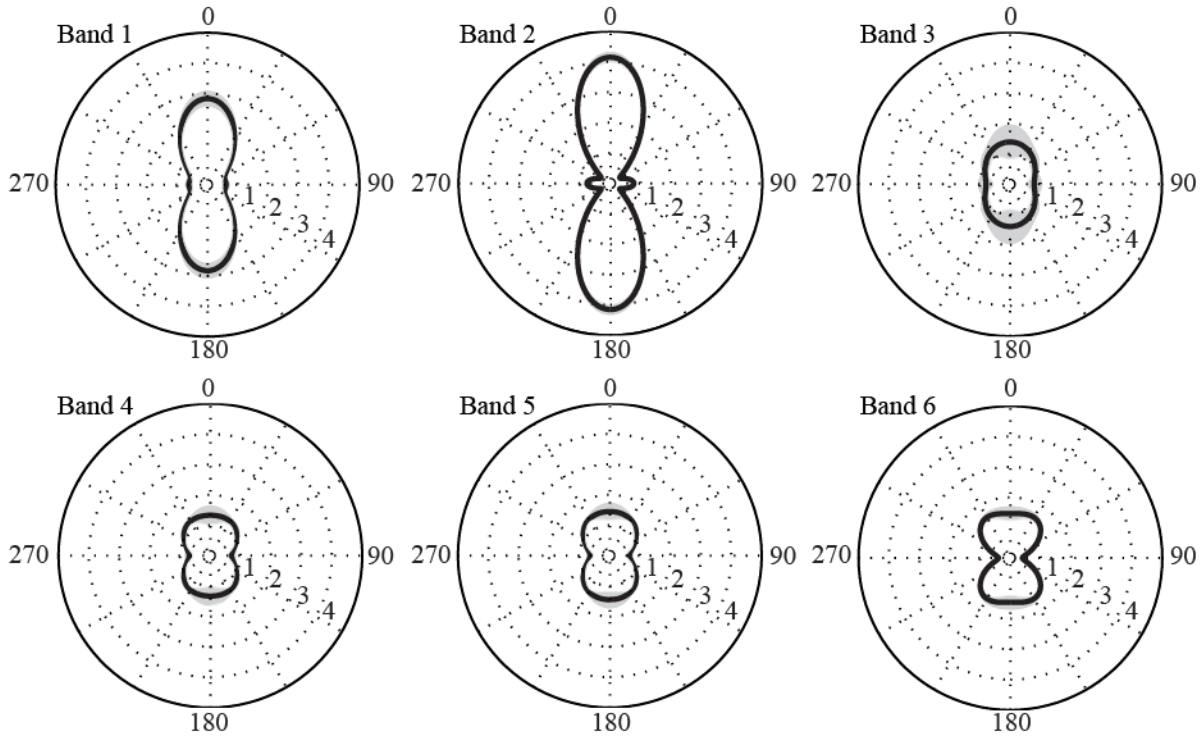

Fig. 4:

Table 1:

Band	Assignment	Binding Energy (eV)	β_2	β_4
1	$4s^1 4p^6(^2S_{1/2})8p^1 \rightarrow 4s^1 4p^6(^2S_{1/2})$	0.50	1.23 ± 0.19	0.60 ± 0.15
2	$4s^1 4p^6(^2S_{1/2})7p^1 \rightarrow 4s^1 4p^6(^2S_{1/2})$	0.73	1.61 ± 0.06	1.54 ± 0.15
3	$4s^2 4p^4 5s^1(^4P_{3/2})6p^1 \rightarrow 4s^2 4p^4 5s^1(^4P_{5/2})$	1.05	0.40 ± 0.38	−0.01 ± 0.41
4	Codling et al. line 15 → $4s^2 4p^4(^3P)5s^1(^4P_{5/2})$	1.22	0.49 ± 0.17	−0.16 ± 0.25
5	$4s^2 4p^4 5s^1(^4P_{5/2}$ and/or $^4P_{3/2})6p^1 \rightarrow 4s^2 4p^4 5s^1(^4P_{5/2}$ and/or $^4P_{3/2})$	1.35	0.60 ± 0.14	−0.15 ± 0.23
6	Codling et al. line 15 → $4s^2 4p^4(^3P)5s^1(^4P_{3/2})$	1.43	0.89 ± 0.18	−0.43 ± 0.13